Peter Lanzer, M.D.
Charles Barta, M.S.E.E.
Elias H. Botvinick, M.D.
Hans U. D. Wiesendanger, D.Sc.
Gunnar Modin, B.S.
Charles B. Higgins, M.D.

ECG-Synchronized Cardiac MR Imaging: Method and Evaluation[1]

An electrocardiographic (ECG) sensing and gating device compatible with a 0.35-tesla (T) magnetic resonance (MR) imager has been developed and used to produce 802 MR images of the heart in 30 patients. The instrument consists of an isolated acquisition module, an electrically floating preamplifier, and a monitor gating module. Two spin-echo images were acquired for each of five, 0.7-cm thick, transaxial sections from the base to the apex of the heart during each ECG-synchronized imaging run. Image quality was assessed in a blind study by two investigators, on a scale from 0 to 3, as diagnostic [2-3] or nondiagnostic [0-1]. There was agreement in 91.4% of their assessments of diagnostic images (68.1% of the images studied). Resolution of heart anatomy on the MR images was adversely affected by prolonged spin-echo time delay, imaging in late diastole, image acquisition at the cardiac apex, irregular triggering, and artifacts. The synchronization of gradient pulses to the ECG at 0.35 T appears safe for patients, permits diagnostic resolution of images, allows image acquisition at distinct points during the cardiac cycle, and enables monitoring of patients during imaging.

Index terms: Electrocardiography (ECG) • Heart, magnetic resonance studies, 51.129 • Images, quality • Magnetic resonance, technology

Radiology 1985; 155:681-686

[1] From the Department of Medicine, Cardiovascular Division; the Department of Radiology (C.B.H.); and the Cardiovascular Research Institute, University of California, San Francisco. Received October 30, 1984; accepted and revision requested November 30; revision received January 7, 1985. This study was supported by grant CA82-N121 from the California Heart Association and by grants from Diasonics NMR, Inc., South San Francisco, and the Fannie Ripple Foundation, Madison, N.J. Dr. Lanzer is supported in part by grant 462/2-2 from Deutsche Forschungsgemeinschaft, Bonn, West Germany, and by the Ciba Foundation. Dr. Botvinick is an Established Investigator of the American Heart Association, with funds contributed by the California Chapter. He is also supported in part by funding from the George D. Smith Fund, San Francisco. Mr. Barta is a member of the Stanford Linear Accelerator Center, Stanford, California. Dr. Wiesendanger is president of Orbiotech International, Inc., Los Altos, California.

MAGNETIC resonance (MR) is an imaging modality that is applicable to the assessment of the cardiovascular system. In conventional MR techniques, imaging sequences are applied repetitively, usually in 0.5- to 2.0-second (sec) intervals, to planar volumes with transaxial, parasagittal, or coronal spatial orientation. Although data sampling per individual imaging sequence requires only a few milliseconds, the number of sequences needed to produce an image encompasses several minutes of sampling. Consequently, when individual imaging sequences are made indiscriminately throughout the cardiac cycle, heterogeneous data are being sampled from random systolic and diastolic phases, resulting in poorly resolved images of the heart (1). Early studies in small animals revealed improved resolution of cardiac anatomy when the heart rate was slowed during nonsynchronized acquisition of images (2). Significant improvement in resolution is achieved when various physiologic signals are used to synchronize the MR imaging sequences with a specific phase of the cardiac cycle (3). We describe an electrocardiograph (ECG) sensing and gating device designed specifically for safe use with patients in the MR imaging environment. The initial results from ECG-synchronized MR studies of the heart in human subjects at 0.35 tesla (T) field strength are presented, and factors that potentially influence the resulting image resolution are identified.

MATERIALS AND METHODS

Study Population

We evaluated 30 consecutive human subjects by ECG-synchronized MR imaging: 21 men and nine women ranging in age from 26 to 98 (mean = 51.3 years), including seven healthy volunteers and 23 patients with various cardiac diseases. Subjects were studied solely to evaluate the MR imaging technique and gave their informed consent. Two patients were removed from the imager because of claustrophobia and could not be evaluated.

Imaging and Triggering Systems

The MR imaging system (Prototype MR Imaging System, Diasonics MRI Division, South San Francisco, Calif.) was operated at 0.35 T. Spin-echo images at time delays of 28 and 56 msec were acquired from 512 consecutive cardiac cycles. In each cycle, a single projection was obtained by an imaging sequence consisting of a train of 90°-τ-180°-τ-180° radiofrequency pulses and a triad of successively applied magnetic-field gradients, oriented in orthogonal planes for encoding and readout of spatial spin distribution (4).

For image reconstruction, we used a two-dimensional Fourier transformation (5). In the synchronized acquisition mode, sequences were triggered either from the upslope of the ECG R-wave or after a manually preset delay. The imaging sequence repetition time (TR) thus equaled the interval length R-R and varied with changes in heart rate. In multisectional interleaved imaging (6), five adjacent sections, 0.7-cm thick and 100-msec apart, were selectively irradiated within each R-R interval.

A diagram of the type of sequencing used in the imaging series is shown in Figure 1. The imaging period for acquisition of all five sections was roughly 500 msec. The signal-acquisition period was 9 msec/spin echo. MR images were obtained in a matrix of 128 vertical × 256 horizontal volume elements

and were displayed in 256 grey shades, with white shades representing tissues with the highest MR signal intensity (7). The total imaging time ranged from 4 to 10 minutes, with a mean of 6.5 minutes, and represented the product of mean R-R interval length and number of imaging sequence repetitions. This is the product of the number of lines along the phase-encoding axis and the number of averages of each line required to optimize the signal-to-noise ratio. The in-plane spatial resolution was 1.7 × 1.7 mm and the axial resolution was 7 mm. An ECG sensing device (Cardiogate-CG 12, Orbiotech International, Los Altos, Calif.) compatible with a 0.35-T MR imager was developed to synchronize the imaging sequences with a specific phase of the cardiac cycle. The system is designed to sense the ECG signal and to generate an MR-sequence triggering pulse. Noise and artifacts induced by the static magnetic field, radiofrequency pulses, and magnetic field gradients inherent in MR imaging are electronically suppressed. To protect the patient from power-line leakage currents, the electrical ECG signal is converted into an optical signal by an isolated acquisition module and is transmitted by a fiber-optic cable. The isolated acquisition module is powered by an internal 6 V battery. In an extremely unlikely situation, a complete breakdown of all critical components of this isolated acquisition module circuit would generate a 2.3-μA current through the electrodes to the patient. Such low-voltage current is far below the threshold of biological hazard (8). Because the voltage induced by the magnetic-field gradients within the ECG loop is also negligible compared with the low voltage induced within the patient's own body, the device appears safe for use in patients.

A block diagram of the entire Cardiogate system is shown in Figure 2. The system utilizes short electrode leads to the patient and consists of an isolated acquisition module, a single fiber-optic cable, an electrically floating preamplifier, and a monitor-gating module. The isolated acquisition module contains high-frequency filters. These reduce the amplitude of high-frequency pulses induced in the electrodes during imaging and also protect against overvoltage. After being filtered, the signal passes to the balanced instrumentation amplifier which contains Field Effect Transistor (FET) amplifiers, gain control, and balancing circuits. The ECG signal of the low level (0.5–2.0 mV AC) and frequency (0.2–80 Hz) is amplified up to a gain of 1,000 without loading the signal source. To isolate the patient from the AC power line, the electrical signal is converted to a light signal in the fiber-optic modulator and transmitter. The light signal is then transmitted by the fiber-optic cable to an electrically floating preamplifier located outside the Faraday cage housing the MR imager. The low-voltage signal is recovered by a fiber-optic receiver and demodulator, transmitted through the overvoltage protection circuit and frequency filter, and amplified. The signal is then converted by the 20-kHz modulator and transferred to the monitor-gating module for further processing, including demodulation and separation from artifacts in a high-gain, high-pass filter and slew rate limiter. Next, an automatic threshold detector and conditioner adjusts the signal amplitude to an appropriate level and generates the rectangular pulse to trigger the imaging sequence from the rising edge of the ECG R-wave.

The output amplitude of the rectangular pulse and the time delay between the ECG R-wave and the trigger pulse are manually adjustable. For synchronization, quality control, and patient monitoring, the recovered ECG signal is displayed on a cathode ray screen and recorded on a strip chart recorder.

NDM Silvon ECG electrodes (NDM Corporation, Dayton, Ohio) are attached to the patient in the right and left subclavicular region and in the midaxillary line at the fifth intercostal space. To minimize DC offset and to improve electrode stability, the skin is cleansed with alcohol, gently

Figure 1

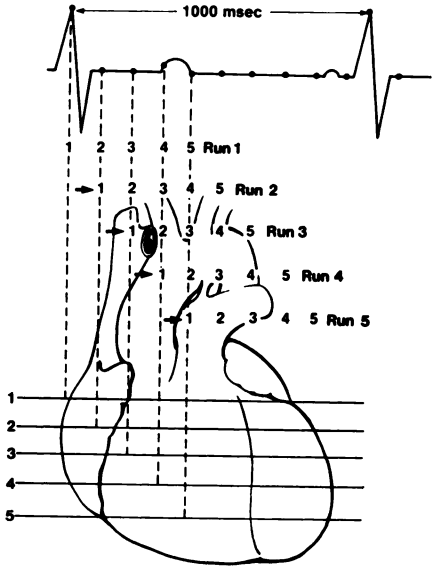

Diagram of multisection imaging of heart shows imaging runs 1 through 5 synchronized with the ECG. Each run encompasses five sequences corresponding to anatomic levels 1–5 shown horizontally below. The first sequence of Run 1 is triggered from the ECG R-wave and corresponds to imaging at anatomic level 1. Subsequent sequences are each offset by 100 msec and 7.0 mm. Thus, at a 60 beat/min heart rate and R-R interval of 100 msec, the fifth sequence of Run 1 images anatomic level 5 at end systole and the fifth sequence of Run 5 gives an image late in the diastolic phase. However, time delay can be preset manually to any value by means of the ECG sensing device.

Figure 2

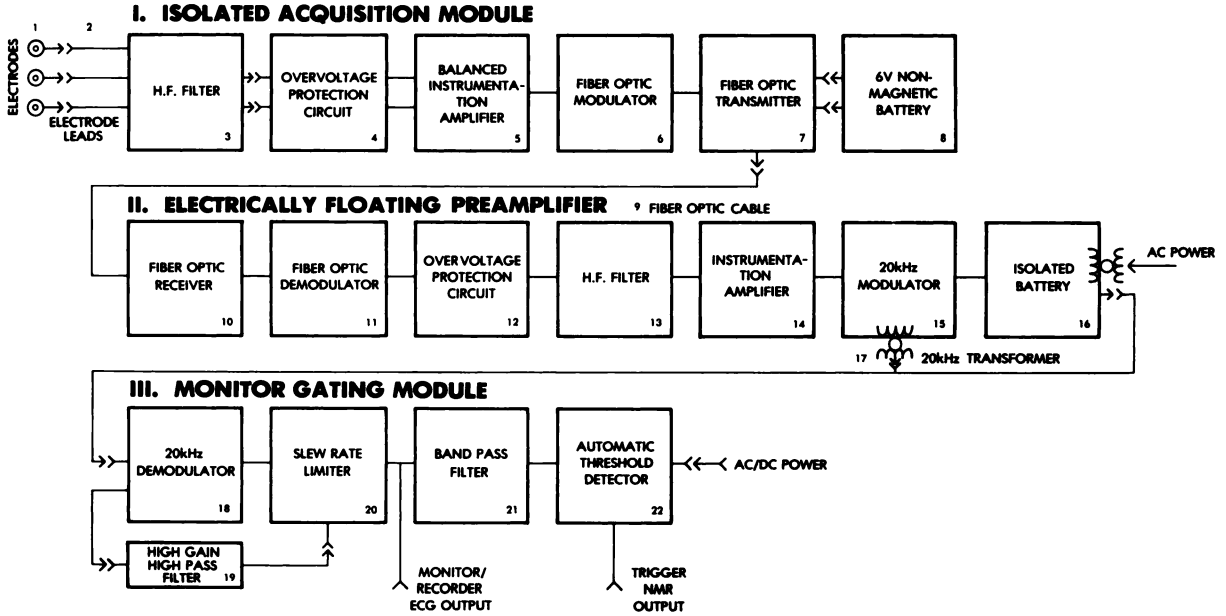

Block diagram of Cardiogate-CG 12 sensing and gating device shows principal parts of the isolated acquisition module (*I*), electrically floating preamplifier (*II*), monitor gating module (*III*), and in-series connected electrodes and electrode leads to the patient.

abraded, and lubricated with conductive jelly. Before imaging, the resistance between skin and electrodes is measured and the ECG signal is monitored to assure signal stability. Typically, skin resistance did not exceed 50,000 ohms. The presence of the NDM Silvon ECG electrodes, patient electrode leads, and isolated acquisition module within the MR imager did not measurably increase background noise levels.

Imaging Protocol

In each patient, the first imaging run was acquired by triggering from the R-wave. One to five additional runs were acquired with a preset delay or after repositioning to a different anatomic level. A total of 64 imaging runs (640 images) were triggered without any preset delay at the ECG R-wave, while 20 imaging runs (200 images) were acquired with a preset delay ranging from 100 to 700 msec between the ECG R-wave and sequence initiation. During each imaging run, the ECG was monitored continuously; it recorded at a paper velocity of 10 mm/sec, with 10-sec intervals at the end of every minute recorded at 25 mm/sec. From the continuous ECG tracings we assessed cardiac rhythm and the frequency of premature ventricular beats, the latter graded according to the criteria of Lown and Graboys (9). The mean heart rate, heart rate variability, and the presence and cause of inconsistent triggering were assessed for each imaging run from 25 mm/sec tracings. Heart-rate variability was measured as the absolute and relative variation in R-R interval during imaging.

Image Analysis

Image quality, determined as the resolution of cardiac anatomy on each image, was assessed visually by two independent investigators and graded as follows: 0 = no cardiac structures resolved, 1 = cardiac structures are poorly resolved, 2 = cardiac structures are apparent but not completely defined, and 3 = cardiac structures are completely and sharply defined. Images graded 0 and 1 were regarded as nondiagnostic; those graded 2 and 3 were regarded as diagnostic. In all images, the presence of band artifacts of variable thickness and intensity was noted.

Resolution quality was then related to the following parameters: spin-echo time delay, timing of image acquisition within systole and diastole, anatomic level, presence of artifacts, and ECG synchronization parameters. For the analysis, systolic and diastolic segments were divided into thirds.

To assess the degree of agreement between the two observers, the contingency coefficient was calculated. Chi-square analysis or, if necessary, Fisher's exact test were used for the univariate analysis of the effect of the individual parameters on image resolution. To ascertain the relative effect of each parameter, a stepwise multiple logistic regression (10) was performed.

Figure 3

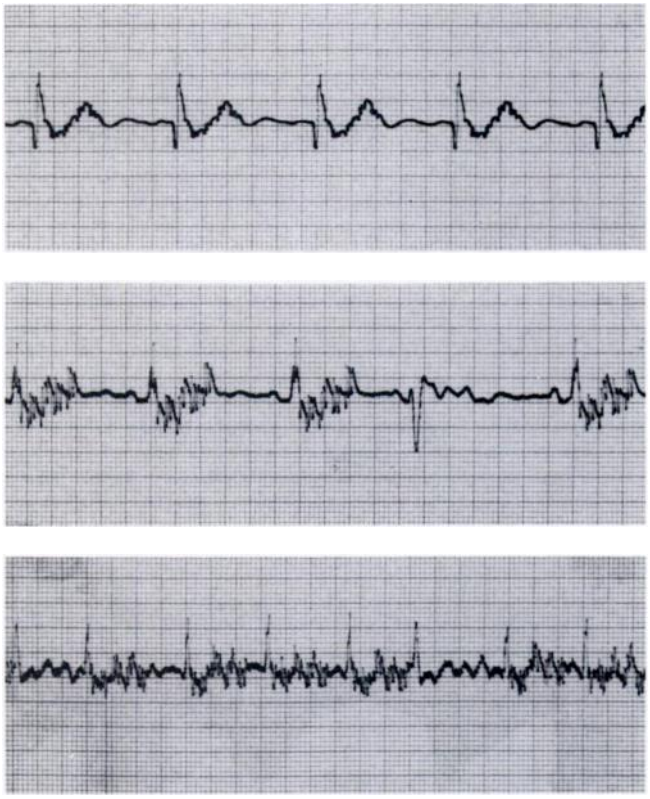

Examples of ECG tracings acquired during MR imaging show (**a**) sinus rhythm, (**b**) Lown grade 1 ventricular extrasystolic beat, and (**c**) atrial fibrillation. The timing of each of the five imaging sequences in Runs 1–5 are inscribed on each tracing.

a. Interfering radiofrequencies are electronically suppressed and original ECG pattern is unmasked. Patient's fifth sequence (at 60 beats/min) coincides with end of T-wave.

b. Variation in TR due to ventricular extrasystolic beats. Because of variable QRS configuration and trigger threshold adjustment, the sequences were sometimes triggered from varying portions of the extrasystolic complexes.

c. Change in R-R interval duration from 500 to 800 msec causes data sampling from various phases of cardiac cycle. Also, during short R-R intervals the last sequence overlaps the following R-wave and causes inconsistent variations in triggering and TR.

RESULTS

ECG Synchronization

A reliable ECG signal was recorded in each subject. The patients reported no unusual sensations, and there were no medical complications during imaging. Twenty-nine patients were in sinus rhythm with normal voltage and without conduction abnormalities. One patient showed atrial fibrillation. Overall, the mean heart rate was 74 beats/min (range: 48–128 beats/min). Variations in heart rate were observed in all imaging runs. For patients in sinus rhythm, heart-rate variations per imaging run ranged from 4 to 12 beats, accounting for a relative R-R variation of 2%–16%. In the patient with atrial fibrillation, the relative R-R variation was 35% per imaging sequence. Lown grade 1 premature extrasystolic heartbeats occurred in eight patients during 14 imaging runs.

Inconsistent triggering occurred in seven patients during 12 imaging runs. This was due either to an inadequate adjustment of the R-wave amplitude and trigger threshold, which resulted in the elimination of one or a series of trigger signals (observed in five patients and ten imaging runs) or to an occasional overlap of imaging sequences with the subsequent R-wave, resulting in the elimination of the trigger signal from the respective cardiac cycle (observed in two patients and two imaging runs). In six imaging runs, three patients with premature contractions simultaneously presented ECG R-wave amplitude maladjustment. The electrocardiograms in Figure 3 were acquired during imaging of three patients and show regular sinus rhythm, ventricular extrasystolic beat, and atrial fibrillation.

Figure 4

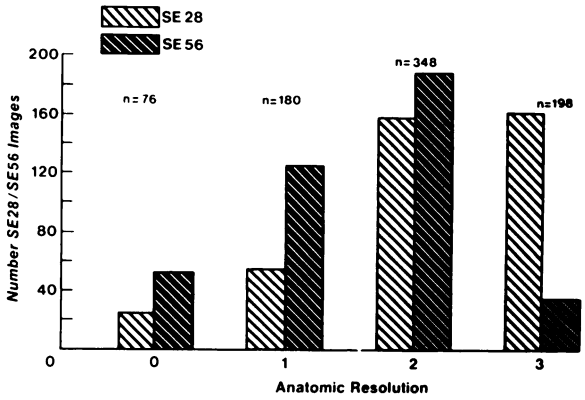

Relationship between image grades 0–3 and spin-echo time delays (TE) of 28 and 56 msec is shown. Grades 2 and 3 are more frequent among 28-msec spin-echo images (TE 28 msec = 322; TE 56 msec = 224); grades 0 and 1 are more frequent among 56-msec spin-echo images (TE 56 msec = 177; TE 28 msec = 79), ($P < .01$).

Figure 5

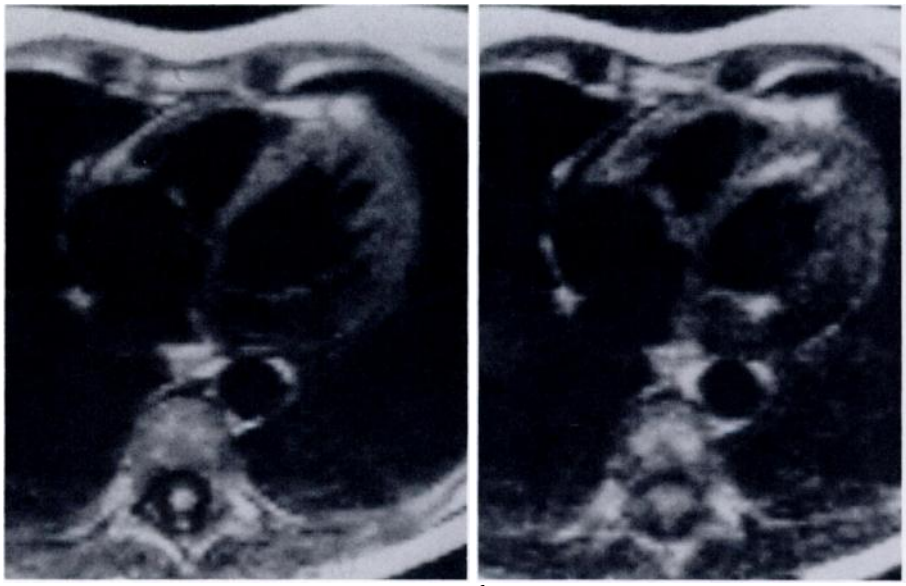

a. b.

Spin-echo images through heart at midventricular level at 28 and 56 msec are shown.
a. Decreased resolution of internal architecture is evident in TE 56-msec image, graded 2.
b. TE 28-msec image was graded 3.

Figure 6

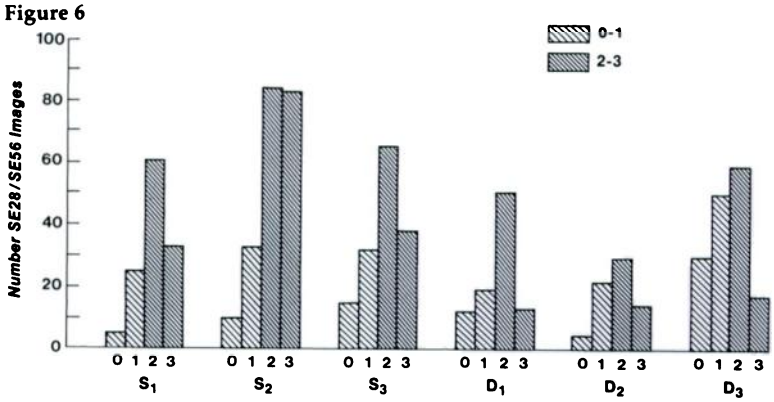

Distribution of image grades 0–3 among early, mid, and late thirds of systole (S_1–S_3) and diastole (D_1–D_3) is shown. Distribution is similar except in late diastolic images (D_3), where there is higher proportion of nondiagnostic grades ($P < .01$).

Image Resolution

Overall, 802 ECG-synchronized MR images of the heart were acquired in 84 imaging runs, including equal numbers of 28- and 56-msec spin-echo studies. Thirty-eight images acquired at distal levels showed only subdiaphragmatic organs. Seventy-six images (9.5) were graded 0; 180 (22.4%) were graded 1; 348 (43.4%) were graded 2; and 198 (24.7%) were graded 3. Both observers agreed on anatomic image resolution in 76.4% of all cardiac images, with a contingency coefficient of 0.86. Both observers agreed in 91.4% of their judgments as to whether images were diagnostic, with a contingency coefficient of 0.81.

The relationship between image grade and spin-echo time delay is shown in Figure 4. Among nondiagnostic studies, the number of 56-msec spin-echo images was significantly higher than the number of 28-msec spin-echo images ($P < .01$). Among diagnostic images, on the other hand, the number of 28-msec images was higher ($P < .01$). Typical examples of both 28- and 56-msec images are shown in Figure 5.

The distribution of image grades among early, mid, and late thirds of systole and diastole are shown in Figure 6. In the last third of diastole there was a significantly greater proportion of nondiagnostic images than in other portions of the cycle ($P < .01$). The sections shown in Figure 7 illustrate the effects of imaging at varying parts of the cardiac cycle.

Anatomic level also affects image quality (Fig. 8). Images acquired at the cardiac apex showed a greater proportion of nondiagnostic ratings than those acquired at other anatomic levels ($P < .01$).

Mean heart rate during acquisition, measures of heart-rate variations, and the presence of Lown grade 1 extrasystolic contractions had no statistically significant relationship to image resolution. Similarly, no significant difference in anatomic resolution was noted in the presence of inconsistent triggering, regardless of cause. However, images without extrasystolic activity and inconsistent triggering were significantly better in resolution ($P < .01$) than images acquired in the presence of these conditions.

In 255 cardiac images, 319 artifacts were noted, 315 (98.7%) of which were identified as horizontal banding of alternating signal intensity across the image. Of these, 262 (82.1%) artifacts were fine, streaky bands and 53 (16.6%) were broader stripes. Four artifacts (1.3%) were from vertical bands of unequal intensity. Overall, there was a

significant difference in anatomic resolution between images without artifacts and those with artifacts present ($P < .01$). Figure 9 shows a typical example of an artifact imaged as fine, streaky bands. In addition, ten images were degraded because of the patient's voluntary motion during imaging.

Analysis

In an attempt to assess the independent effect of individual parameters negatively influencing image resolution, a multivariant logistic regression analysis was performed, with results summarized in Table 1. Imaging at the apex, the presence of artifacts, long spin-echo time delays, and inconsistent triggering with extrasystolic beats were the most prominent factors leading to poor anatomic resolution in the images. Because of the sparsity of observations in some subgroups, imaging in late diastole was not a predictive variable.

DISCUSSION

In earlier studies, poor anatomic resolution of nonsynchronized MR images of the beating heart was attributed to acquisition of data from systolic and diastolic phases of the cardiac cycle (1, 2). Although various physiologic signals have been utilized to achieve synchronization, distinct advantages of synchronization to the electrocardiogram have been demonstrated (3). In this study, ECG synchronization of imaging sequences was utilized exclusively, and the quality of the resulting cardiac images was assessed.

Electrocardiograms, acquired with a sensing device designed for safe use in the MR environment, were obtained from all patients without complications. Although an artifact accompanies the application of each imaging sequence, the underlying P-QRS-T configuration can be observed in most patients. Further improvement in the quality of the ECGs appears possible by improved electronic suppression of radiofrequency pulses. Reliable triggering signals were produced in all but seven patients. In five of these patients a consistent trigger signal was produced subsequently by amplification of R-wave amplitude. Low-voltage R-waves can nevertheless prevent proper triggering by failing to reach the sensing threshold of the system. In the patient whose images showed sequence overlap, consistent triggering was accomplished by decreasing the preset delay to values where all sequences were fitted within the limits of the R-R interval. In the remaining patient, who had a mean heart rate of 126 beats/min corresponding to an R-R interval of 476 msec, most sequences of the fifth section overlapped the subsequent R-wave, resulting in data acquisition from every other heartbeat.

In this initial evaluation, 68% of the cardiac images were of sufficient quality for the investigators to resolve cardiac anatomy, but resolution varied among specific subgroups of imaging conditions. For example, nondiagnostic images were acquired more frequently with 56-msec spin-echo delay during late diastole and at the cardiac apex.

The adverse effect of a longer spin-

Figure 7

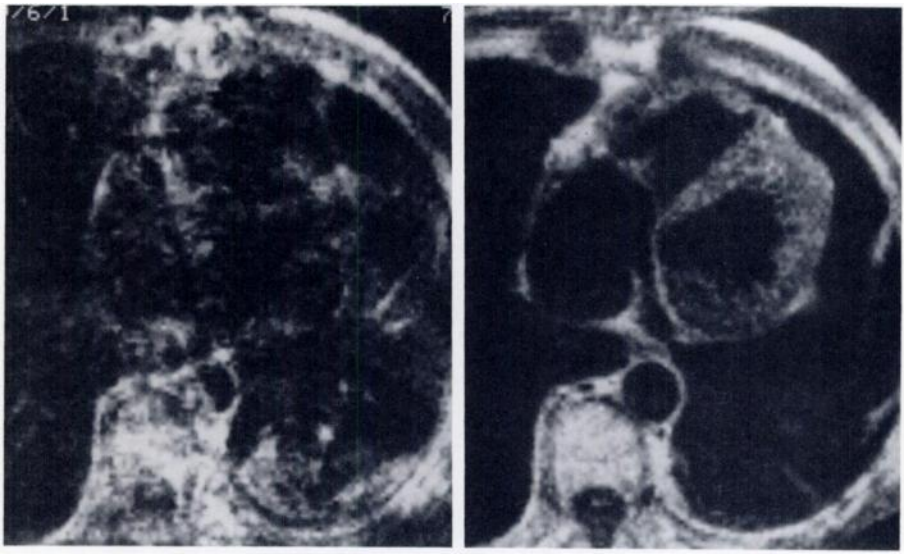

a. b.

Two TE 28-msec spin-echo images from a similar anatomic level acquired in end diastole (**a**) and late systole (**b**) during a single imaging run are shown. Virtually no cardiac structures are seen in diastolic image, graded 0; cardiac anatomy seems well resolved in systolic image, graded 3.

Figure 8

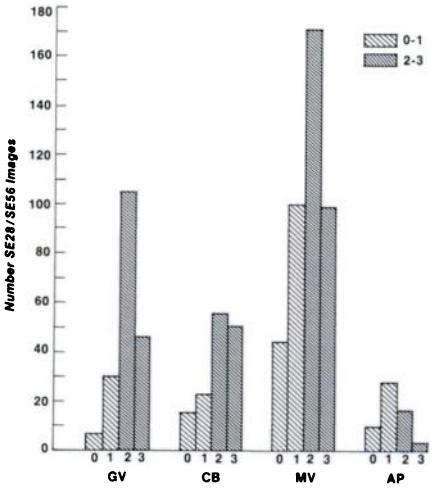

Frequencies of grades 0–3 at anatomic levels corresponding to the great vessels (*GV*), cardiac base (*CB*), mid-ventricles (*MV*), and apex (*AP*) show no difference in distribution except for images acquired at cardiac apex, which have higher proportion of grades 0 and 1 ($P < .01$).

Figure 9

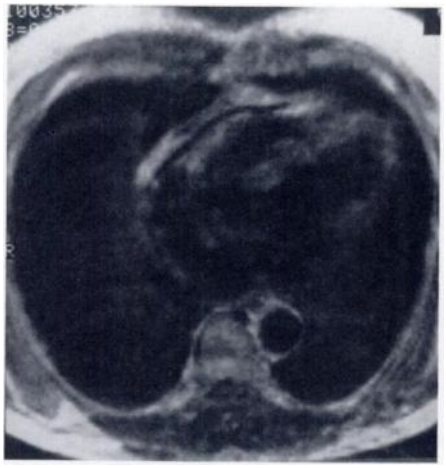

Example of TE 28-msec spin-echo image with reduced resolution of cardiac anatomy from narrow-band artifacts. Cardiac structures appear blurred and irregular (graded 1). Artifacts may represent frequent respiration during imaging.

Table 1
Influence of Parameters on Prediction of Image Quality

Parameter	Coefficient	Standard Error	Coefficient of SE
Imaging apex	1.096	0.173	6.348
Image artifacts	0.810	0.096	8.424
Spin-echo delay	0.729	0.097	7.518
Inconsistent trigger	0.622	0.101	6.155

Note.—In this multivariant analysis, the coefficients, standard errors, and their ratios indicate the relative weight of the parameters in the prediction of poor image quality. The highest predictive value for resolution of nondiagnostic images corresponded to imaging at the apex of the heart.

echo delay likely relates to a greater loss of signal intensity because of more extensive cardiac motion out of the imaging plane between the 90° pulse and spin-echo acquisition as well as to a more complete decay of the transverse magnetization with increasing time delay. The low anatomic resolution in late diastole may relate to the higher sensitivity of the late diastolic filling phase to variations in R–R intervals and, if present, to intermittent data acquisition from early systolic phases of the subsequent cycle (3). In addition, increase in signal intensity from slow flow (7) may obscure vascular and cavitary interfaces during late diastole (11) and contribute to decreased anatomic resolution. Reduced resolution at the apex may reflect the respiratory motion of the diaphragm.

No difference in image quality was observed at heart rates ranging from 48 to 128 beats/min. This suggests that variations in wall-motion velocity at heart rates up to 128 beats/min do not affect the 9-msec spin-echo acquisition while the readout gradient is applied. Inconstant TRs were introduced by changes in heart rate, extrasystolic beats, and inconsistent triggering.

The lack of significant differences in resolution between images acquired across a spectrum of R–R intervals suggests that moderate TR variability does not alter anatomic resolution. However, more prominent changes in TR resulting from extrasystolic heartbeats and inconsistent triggering may affect anatomic image resolution adversely by producing variations in magnitude of the longitudinal and transverse magnetization among individual projections with a consecutive distortion of the Fourier reconstruction.

Artifacts were noted in 32% of the cardiac images. Their presence significantly affected resolution. Signal variation along the phase-encoding direction or vertical image axis can be produced experimentally by periodic object displacement between individual imaging sequences (12). Similarly, frequent breathing, although spatially more complex, may simulate vertical displacement of anatomic structures between projections and cause frequency distortion of Fourier spectra and consecutive artifact formation. Vertical variations in signal intensity, noted only in four images, appeared related to patient positioning within the coil of the MR imager. Because the field of the radiofrequency coil is most uniform at its center, positioning the patient off center will produce heterogeneous signal induction and consecutive variation in signal intensity across the image. Voluntary motion by the patient during imaging clearly causes a deterioration in anatomic resolution.

The ECG sensing device employed here can be safely used in patients for triggering MR imaging sequences and permitting simultaneous monitoring. A subsequent study (13) demonstrated only minor reversible effects of the magnetic field on the configuration of the ECG pattern in patients. Although the yield of diagnostic images with the device is high, prolonged spin-echo time delay, inconsistent triggering, imaging late diastole, and imaging at the cardiac apex may limit the resolution of cardiac anatomy. ■

Correspondence and reprints: Peter Lanzer, M.D., 1186-Moffitt, University of California, 505 Parnassus Avenue, San Francisco, CA 94143.

References

1. Hawkes RC, Holland GN, Moore WS, Roebuck EJ, Worthington BS. Nuclear magnetic resonance (NMR) tomography of the normal heart. J Comput Assist Tomog 1981; 5:605–612.
2. Schiller NB, Botvinick E, Davis P, Engelstad B, Lanzer P, Kaufman L. Nuclear magnetic resonance imaging of the guinea pig heart (abstr.). J Amer Coll Cardiol 1983; 1:617.
3. Lanzer P, Botvinick EH, Schiller NB, et al. Cardiac imaging using gated magnetic resonance. Radiology 1984; 150:121–127.
4. Edelstein WA, Hutchinson JMS, Johnson G, Redpath T. Spin warp NMR imaging and applications to human whole-body imaging. Phys Med Biol 1980; 25:751–756.
5. Kumar A, Welti D, Ernst RR. NMR Fourier zeugmatography. J Magnet Res 1975; 18: 69–76.
6. Crooks L, Hoenninger JC, Arakawa M. Method and apparatus for rapid NMR imaging of nuclear densities within an object. U.S. Patent 4,318,043 (March 2, 1982).
7. Crooks LE, Mills CM, Davis PL, et al. Visualization of cerebral and vascular abnormalities by NMR imaging: the effects of imaging parameters on contrast. Radiology 1982; 144:843–852.
8. Saunders RD, Orr JS. Biologic effects of NMR. In: Partain CL, James AE, Rollo FD, Price RR, eds. Nuclear magnetic resonance: NMR imaging. Philadelphia: Saunders, 1983; 383–396.
9. Lown B, Graboys TB. Management of patients with malignant ventricular arrhythmias. Am J Cardiol 1977; 39:910–918.
10. Dixon WJ, ed. BMDP statistical software. Berkeley: University of California Press, 1981.
11. Lanzer P, Botvinick E, Schiller N, et al. Analysis of variation in vascular luminal nuclear magnetic resonance signal intensity during the cardiac cycle (abstr.). J Amer Coll Cardiol 1984; 3:539.
12. Wood M, Henkelman RM. NMR image artifacts from periodic motion (abstr.). In: Proceedings of the Society of Magnetic Resonance in Medicine, San Francisco, August 16–19, 1983; p. 380.
13. Lanzer P, Botvinick E, Schiller N, Higgins C. The influence of a 0.35 T static magnetic field on the electrocardiograms of humans (abstr.). J Amer Coll Cardiol 1984; 3:539.